Surface & Coatings Technology 466 (2023) 129639

Contents lists available at ScienceDirect

Surface & Coatings Technology

journal homepage: www.elsevier.com/locate/surfcoat

Full length article

Simulation and experimental study on cold sprayed W—Cu composite with high retainability of W using core-shell powder

Nan Deng [a,b,1], Dandan Qu [c,1], Kun Zhang [c,d], Guoliang Liu [d], Shaofu Li [e], Zhangjian Zhou [b,*]

[a] Engineering Research Center of Conducting Materials and Composite Technology, Ministry of Education, Shaanxi Key Laboratory of Electrical Materials and Infiltration Technology, School of Materials Science and Engineering, Xi'an University of Technology, Xi'an 710048, China
[b] School of Materials Science and Engineering, University of Science and Technology Beijing, Beijing 100083, China
[c] Wide Range Flight Engineering Science and Application Center, Institute of Mechanics, Chinese Academy of Sciences, Beijing 100190, China
[d] School of Engineering Science, University of Chinese Academy of Sciences, Beijing 100049, China
[e] State key Laboratory of Multiphase Complex Systems, Institute of Process Engineering, Chinese Academy Science, Beijing 100190, China

ARTICLE INFO

Keywords:
Core-shell powder
W-cu composite
Cold spray
Three-dimensional finite element model

ABSTRACT

A W—Cu composite coating with high W retention was fabricated by cold spraying using a novel W@Cu core-shell powder. The impact and deposition mechanism of W@Cu core-shell powder during cold spraying were investigated using finite element modeling in comparison to typical W—Cu satellite powder. The results revealed that the W@Cu core-shell powder shows non-local strain and dispersive residual stress in the final coating, resulting in a low rebound energy and interfacial bonding energy. As a result of employing the core-shell powder, a cold-sprayed W—Cu composite coating with a high W content can be prepared, and the coating has a non-pancake-like layer morphology. After optimizing the core-shell powder with a Ni transition layer, the final coating demonstrated super-high W retention (98.3 %) and decreased bulk porosity (1 %).

1. Introduction

W—Cu composite materials with excellent thermal and electrical conductivity, as well as mechanical properties are widely used as heat sink materials for thermal management in microelectronics fields and high heat flux component in a fusion reactor, armor-piercing materials in military applications, and electrical contact materials for circuit breaker core components [1,2]. Infiltration, active liquid-phase sintering, and liquid-phase sintering are typical methods for producing W—Cu composites [3–5]. However, these procedures often need high sintering temperatures and lengthy processing times. Hence, it is important to investigate innovative fabrication procedures for producing W—Cu composites with low energy consumption and cost.

As a novel additive manufacturing technology, cold spraying (CS) has significant applications in surface functionalization, composite fabrication, and component reparation [6]. The CS has much lower operating temperature, oxygen concentration, and porosity than traditional thermal spraying coating [7], making it a viable approach for fast prototyping of W—Cu composites. Some simulated and experimental studies revealed that successful cold spray deposition is dependent on adiabatic shear instabilities at the interface between the impacting particle and the substrate during cold spraying, and the particle has a 'jet-like' shape [8]. The interaction of strong pressure waves with the free surfaces at the particle edges, according to the hypothesis, may generate hydrodynamic plasticity. The hydrodynamic plasticity impacts bonding without necessitating adiabatic shear instability [9]. The subject has sparked fierce discussion [10,11]. However, a large amount of plastic deformation occurs in a time span of less than 100 ns during a cold spraying process, which makes that the whole deformation history is very difficult to observe. Therefore, computational simulation is widely used to get an insight to the dynamics of the deformation process. For instance, the impact of copper particles onto a stainless steel substrate including modeling flattening ratios and crater depths [12], the effects of initial particle or substrate temperature and heat conduction on the behavior of copper-on-copper and copper-on-steel impacts [13], as well as the main factors affecting bonding features for several particle material systems [14,15]. Three typical numerical methods were evaluated and the Coupled Eulerian Lagrangian (CEL) has an advantage over the others due to avoidance of excessive mesh distortion and unrealistic deformed shape. In addition, the numerical results by the CEL method

* Corresponding author.
E-mail address: zhouzhj@mater.ustb.edu.cn (Z. Zhou).
[1] Nan Deng and Dandan Qu contributed equally to this work.

https://doi.org/10.1016/j.surfcoat.2023.129639
Received 11 March 2023; Received in revised form 12 May 2023; Accepted 13 May 2023
Available online 20 May 2023

also showed a fairly good agreement with the experiments [16].

The bonding process among particles or between particles and substrate are mostly dominated by metallurgical bonding and mechanical interlocking in pure metal coating, particularly ductile metals [8,17]. Non-ductile metals are often used as coating tamping phase to increase mechanical interlocking force and coating's density. It is not a suited method for cold spraying if the content of non-ductile metal is too high or even 100 % content of non-ductile metal [18], since non-ductile particles with lower deformability are difficult to create excellent mechanical interlocking. Non-ductile materials may be deposited by increasing the cold spraying pressure (3–4.4 MPa) and utilizing helium as the carrier gas. However, the cost is too expensive [19]. The coating's thickness and density are restricted owing to particle rebound produced by excessive kinetic energy [20].

Ductile metals as a binder phase make low-pressure cold spraying of non-ductile metals possible [21], such as W-based or WC-based composites [22,23,25]. However, there is still a problem of limited W or WC phase retention in cold-sprayed coating due to inadequate kinetic energy [22–25]. The W content of the final coating is often substantially lower than that of the original design. As a result, the satellite and core-shell powder were employed as raw materials for cold spraying to increase the non-ductile phase retention rate [26–32]. W—Cu satellite composite powder was employed as basic material in our prior study [25]. Unfortunately, the retention rate of the W phase was still not optimal, being almost equal to zero in a sample containing originally 70 % (fraction of mass) W. Therefore, the aims of this work are to (1) simulate the deposition behavior of innovative W@Cu core-shell powder against typical mechanical mixed W—Cu satellite powder and (2) investigate the production and optimization process of high W retention coating at low pressure.

2. Simulation and experiment

2.1. Detail of simulation

Finite element analysis (FEA) software ABAQUS/Explicit was used for numerical simulation. A three-dimensional model coupled with the Eulerian-Lagrangian method (CEL) was used to study the deformation, deposition, and impact behavior of particles during the spraying process. This work used an eight-node hexahedral element with reduced integration and stiffness hourglass control (C3D8R) as the substrate's meshing element type and transition mesh to reduce the calculation time. In the simulation, the upper face only allowed vertical movement, while the bottom was fixed in all directions as the boundary condition. For particles, an eight-node linear Euler brick element (EC3D8R) with reduced integral points was used for mesh partitioning. In addition, the particle impacted vertically onto the substrate in the current simulation.

The diameter of W@Cu core-shell powder was set to be 15 μm in total, with the diameter of W core 10 μm corresponding to the average size of the sprayed powder particles. The diameters of core Cu particles of satellite powders vary from 15 to 35 μm with Gaussian distribution to keep the same weight ratio. The average W particle size for satellite powders was 3 μm. The particles with above mentioned dimension were drawed in a software named solidworks and treated in an Eulerian domain. Materials could mix together and the interface between materials in the CEL model is undistinguishable. The interface properties of both materials were defined to be general contact. To reduce the computational effort and maintain numerical accuracy, the mesh element size was set to 0.6 μm at the impact center and gradually increased at the edge of the part. The Mie-Gruneisen equation of state and Johnson-Cook plasticity model were used to simulate the elastic and plastic behavior of the particles and substrates. All the material properties were taken from the literature [33–35] and are provided in Table 1.

2.2. Raw material and cold spray processing

Fig. 1 shows schematic of the cold spraying process and raw material. W—Cu satellite powder and W@Cu core-shell powder were used as raw materials. As starting materials for satellite powder, commercially available W (with an average particle size of 3 μm and a purity level of 99.99 %) and spherical Cu powders (with a particle size range of 15–53 μm and a purity level of 99.9 %) were mixed in a V-type blender mixer for 15 h at a weight ratio of 7:3 (Fig. 1(b)). Intermittent electrodeposition was used to fabricate Cu-coated W powders (W@27.25 wt%Cu) with a shell thickness of 2.5 μm and W@6.3 wt%Ni@22.5 wt%Cu powders with a total shell thickness of 2.8 μm (Fig. 1(c)).

The composite coating was fabricated by cold spraying (Beijing Tianchengyu New Material Technology Co., Ltd.). In this process, the preheating temperature of the propelling gas was 500 °C to facilitate the plastic deformation of the raw material. The preheated powder was sprayed on a 6061Al substrate (100 × 50 × 5 mm^3) by accelerating air gas at 2 MPa pressure in a converging-diverging de Laval-type nozzle.

2.3. Characterization

The microstructure of the powder and the coating were observed by scanning electron microscope (SEM) equipped with energy-dispersive spectroscopy (EDS) (JSM-7001F) and electron backscattered diffraction (EBSD). High-resolution transmission electron microscope (HRTEM) were examined by a FEI TECNAL G2 F20 microscope, equipped with energy-dispersive spectroscopy (EDS, Bruker, Xflash Detector 5030). Samples for HRTEM analysis were extracted using focused ion beam (FIB) microscopy. The phase composition of composite coating was detected by performing X-ray diffraction (XRD, SmartLab 9 kW) with a radiation of Cu Ka (the X-ray wavelength was 1.5418 Å, and the tube voltage and tube current were 45 kV and 200 mA, respectively). The retention rate of W was the ratio of the W content in the coating to the W content in the original powder (detected by the Image Analysis software). The 3D microstructural characterization of sample was examined by radiographic technique, X-ray micro-computed tomography (μ-CT, Xradia 520 Versa system, Zeiss, USA) at a voltage of 120 kV. 3D reconstructed images were processed using Dragonfly Pro software. The detail of the X-Ray micro-computed tomography tester: The sample

Table 1
material properties used in the FEA.

Properties	Parameter (unit)	Copper	Tungsten	Al6061
General	Density, $\rho(kg/m^3)$	8900	19,350	2700
	Specific heat, $C_P(J/Kg \bullet K)$	383	130	890
	Thermal conductivity$(W/m \bullet K)$	386.5	174	155
	Melting temperature,$T_m(K)$	1356	3683	925
	Inelastic heat fraction,β	0.9	0.9	0.9
Elastic	Elastic modulus, GPa	124	411	69.1
	Poisson's ratio	0.34	0.28	0.33
Johnson-Cook plasticity parameters	A, B, n, c, m $(MPa$, $MPa)$	90,292,0.31,0.025,1.09	91.711,235.8226,0.2557,0.0461,0.5485	148.4345.5,0.183,0.001,0.895
	Reference strain rate,$\dot{\varepsilon}_0(1/S)$	1	0.001	597.2
	Reference temperature,$T_{ref}(K)$	298	1523	294

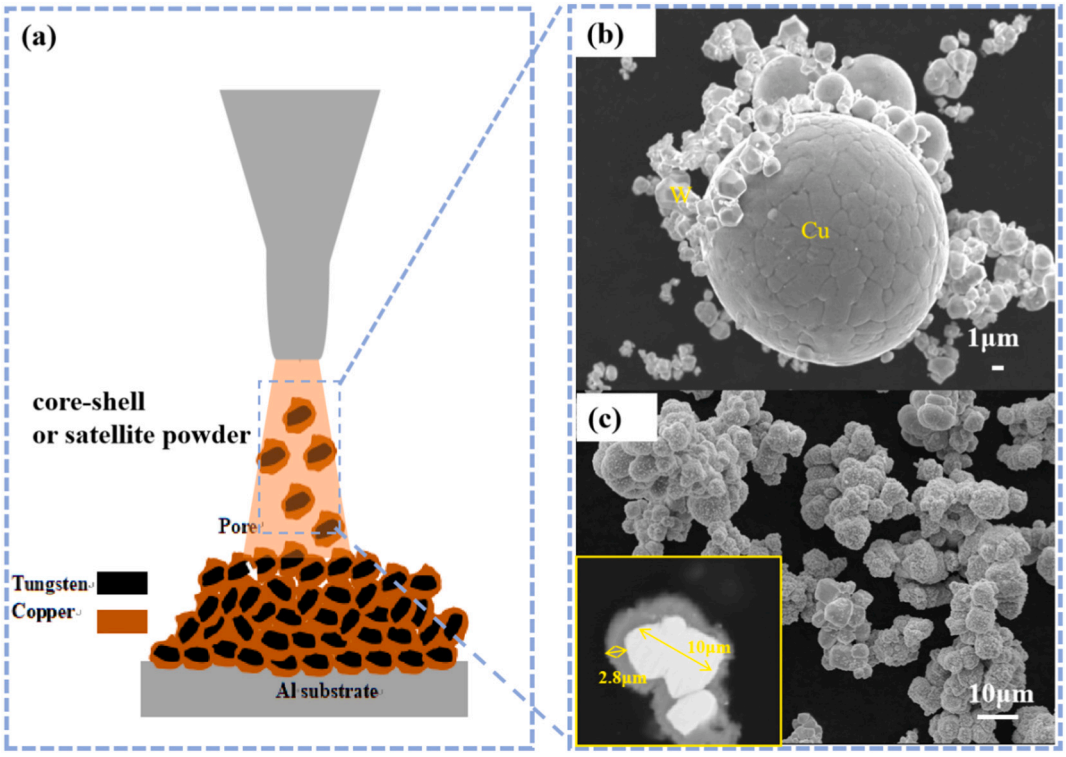

Fig. 1. (a) Overall schematic illustrations of the cold spraying process, the SEM images of (b) W—Cu satellite powder and (c) W@Cu core-shell powder (The inserted image is the cross section of the W@Cu core-shell powder).

size was 3 × 5 × 6 mm, the volume resolution was 3.0 μm, the input energy and power were 120 KV and 10 W, the field of view was φ3 × 3 mm, and the scanning time was about 3–4 h.

3. Results and discussion

3.1. The impact behavior of single particle

Fig. 2 shows the simulation results of the plastic deformation process of a single W—Cu satellite particle and a W@Cu core-shell particle. In a nanosecond period, both composite powders impacted the substrate, specifically, the plastic deformation process of a satellite particle and its substrate during the impact with the interval time 30 ns are showed respectively in Fig. 2(a1 ~ e1) and (f1 ~ j1). Meanwhile, the plastic deformation process of a core-shell particle and its substrate during the impact with the interval time 10 ns are showed respectively in Fig. 2(a2 ~ e2) and (f2 ~ j2). The shape of the W—Cu satellite powder is flattened, with the greatest plastic deformation occurring in the Cu core and particle's contact area with the Al substrate, as seen in Fig. 2(a1 ~ e1, f1 ~ j1). As shown in Fig. 2(a2 ~ e2, f2 ~ j2), the deformation in the W@Cu core-shell powder occurred at the interface between the Cu shell and the substrate, with little deformation in the W core. The Cu shell of the core-shell powders which can be distinguished by eulerian volume fraction (EVF) during the post-processing of the simulation, as seen in Fig. S1. The Cu shell of the core-shell powder has a 'jet-like' shape, and the W shell restricts the 'jet-like' formation of ductile Cu for satellite powder. It was found that both powders' variable core and shell components cause differences in the microstructure and characteristics of the coating. Furthermore, a W core and Cu shell satellite composite particle was formed using W powder with a diameter of 10 μm and Cu powder with a diameter of 4 μm as raw materials. The microstructure of composite coating is shown in Fig. S4. W particles are distributed throughout the Cu matrix, suggesting that the Cu and W in this raw material cannot form the above-mentioned a W core and Cu shell composite particle. It also demonstrated the superiority and uniqueness of W@Cu core-shell powder, which was employed in this investigation. Because of the high density of the single particle, the W@Cu core-shell powder caused massive plastic deformation in the substrate (Fig. 2(j1, j2)).

3.2. Characterization and optimization of W—Cu composite coatings

Fig. 3 represents the fabricated coating's microstructure and Lagrangian-Eulerian finite element simulation. The coating thickness of the W—Cu satellite powder was only tens of microns, but that of W@Cu core-shell powder can achieve millimeter-level. The satellite powder coating has a typical lamella microstructure, as shown in Fig. 3(a), which demonstrates a zonal distribution characteristic of W and Cu. The darker areas and whiter areas are copper rich and tungsten rich, respectively. Interestingly, the distribution of W and Cu in the W@Cu core-shell powder coating is comparable to the morphology of a sintered sample rather than a typical sprayed coating, as seen in Fig. 3. (b). The enlarged images of W@Cu core-shell powder coating with map scanning are given in Fig. S5. The coating's key components are the elements of copper and tungsten. Carbon is also identified in the hole as a residual polishing ingredient following diamond polishing paste polishing. The following factors contribute to the formation of holes in the coating: (1) inadequate mixture of Cu and Cu; and (2) exfoliation of W particles due to poor bonding.

Fig. S2 shows eulerian volume fraction (EVF) of copper and tungsten during simulation of the satellite powder coating in Fig. 3 (c). Fig. S3 shows EVF of copper and tungsten during simulation of the core-shell powder coating in Fig. 3 (d). All the stress concentrations in both composite coatings occur in W particles (as shown in Fig. 3(c, d)). For the coating, a strip of localized deformation is created inside the Cu phase, which may facilitate the creation of several shear bands to release the kinetic energy. Nonlocalized strain and dispersive residual stresses occur in the coating of W@Cu core-shell powder, which may be an explanation of the non-pancake-like layer shape (Fig. 3(b)). Previous research [36] has declared that the compression ratio, R, may be used to

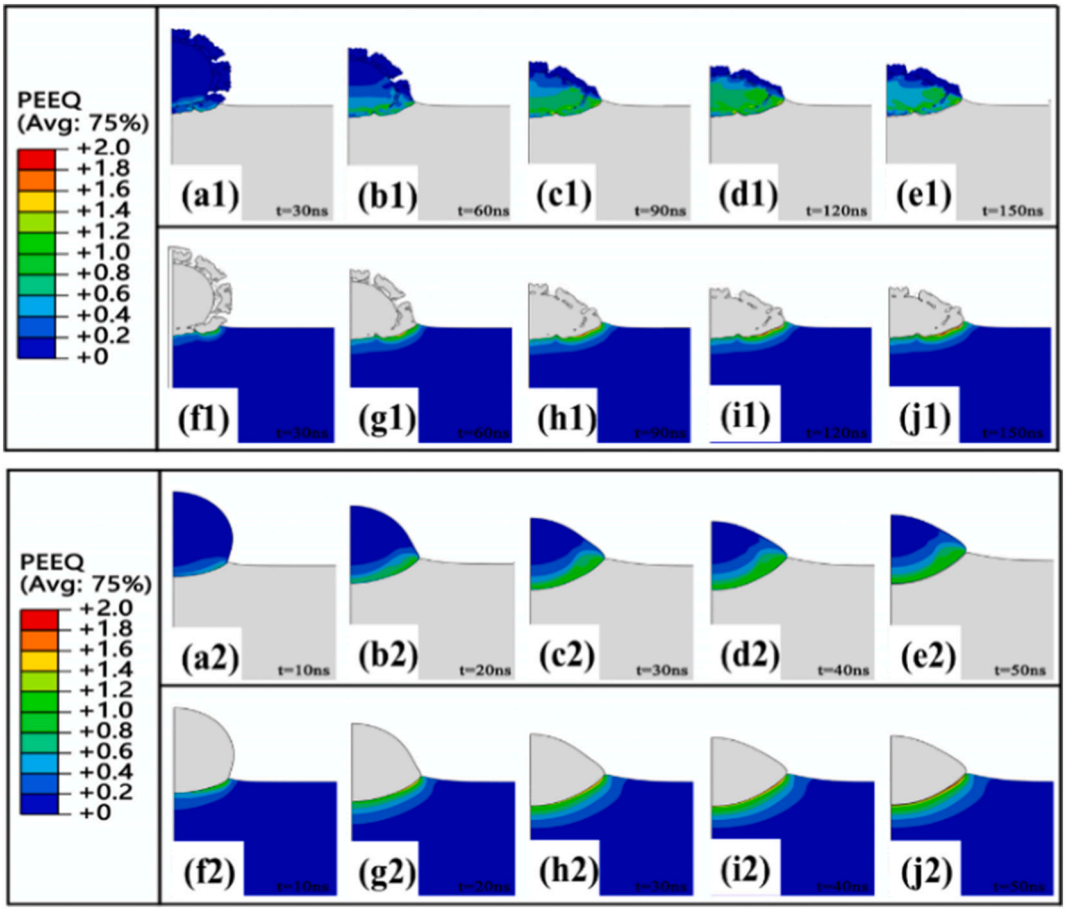

Fig. 2. Lagrangian-Eulerian finite element simulation of the plastic deformation process during impacting of the single composite particle: (a1) ~ (j1) using W—Cu satellite powder, (a2) ~ (j2) using W@Cu core-shell powder (PEEQ: Equivalent plastic strain).

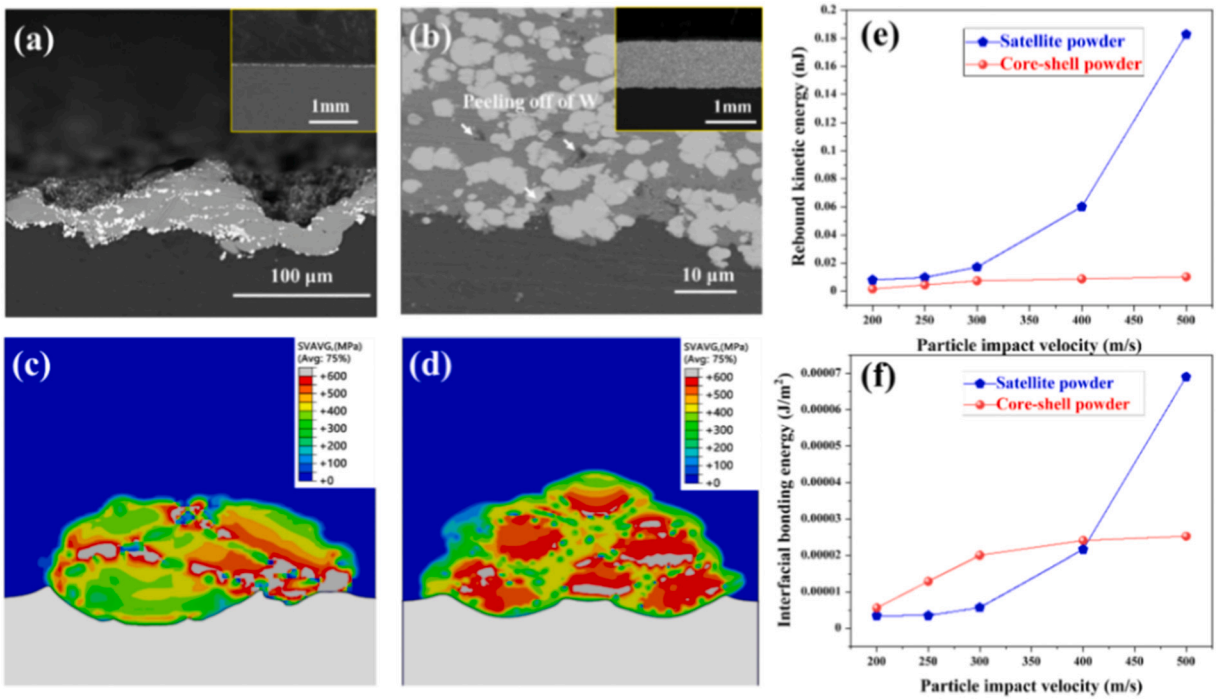

Fig. 3. Microstructure and Lagrangian-Eulerian finite element simulation of the coating: (a) and (c) the W-30 wt% Cu coating by W—Cu satellite powder, (b) and (d) the W-27.25 wt%Cu coating by W@Cu core-shell powder (The inserted pictures were the overall picture of the coating), (e) and (f) the rebound kinetic energy and the interfacial bonding energy at different particle impact velocities.

describe total particle deformation following impact. It can be calculated by $R = \frac{d_0 - h}{d_0}$, Where d_0 is the diameter of particle before deforming, and h is the height of the particle after deformation. The compression ratio of the W—Cu satellite powder coating is 0.6–0.8, which suggests that it is flattened (as seen in Fig. S8). The compression ratio of the W@Cu core-shell powder coating performs the reverses (0.15), with a penetrated substrate and fewer deformed particles. It illustrates that the deformation of the particle is not a typical prerequisite for the successful bonding of non-ductile coating with the soft phase. Furthermore, the simulation can provide the rebound energy and interfacial bonding energy of various powder types to further elucidate the mechanism of coating formation, as shown in Fig. 3(e, f). The rebound energy [37] is defined as kE_R, $kE_R = \frac{1}{2} m_p V_R^2$, Where m_p is the particle mass and V_R is the particle vertical rebound velocity. In this study, the interfacial cohesive strength is defined as zero. The interfacial bonding energy, $\frac{kE_R}{A_c}$, can be determined from the simulations with zero interfacial bonding strength, Where A_c is the contact area. The $\frac{kE_R}{A_c}$ ratio is interpreted as a lower bound of the interfacial bonding energy for the interface to remain bonded. In the case of the W—Cu satellite, the rebound energy and interfacial bonding energy are found to be a quadratic function of particle impact velocity. When the velocity is less than 400 m/s, W—Cu satellite powder has a lower interface bonding energy than W@Cu core-shell powder due to the significant mechanical interlocking effect. However, when the particle impact velocity rises, the W—Cu satellite powder bounces, increasing the interface bonding energy and rebound energy. This is not the case with the W@Cu core-shell powder. In all particle impact velocities, the rebound energy of the W@Cu core-shell powder is lower than that of the W—Cu satellite powder. The rebound energy and interface energy grow and then stabilize as the particle impact velocity increases. This is due to the Cu shell producing plastic deformation and the W core tamping the coating, resulting in muscular bonding strength and low rebound energy, as described in reference [38].

The simulation results reveal that there is obvious plastic strain at the W and Cu phases, resulting in a stress mismatch at the interface for the W@Cu core-shell powder. The experimental results show that the mismatch is responsible for the exfoliation of W particles (Fig. 3(b)). Similarly, the weakest areas in a cold sprayed CuNiDiam-Al coating by CuNi-coated diamond powders are found to be at the internal Ni-diamond interfaces or the diamond cores [38]. Heat treatment of cold-sprayed samples has been proven in studies [39–42] to successfully reduce or remove work hardening and dynamic flaws induced by deformed particles via recovery and recrystallization. Diffusion between atoms increases the bonding between particles. However, due to insolubility of W and Cu, the pore created by exfoliation of W particles cannot be eliminated. As a result, in order to enhance interface bonding strength, a Ni interlayer is added between W and Cu in the optimized W@Cu core-shell powder. The surface morphology and map scanning of the W-(Ni)-Cu coating before and after heat treatment are shown in Fig. 4 (a) and (b). In the W-(Ni)-Cu coating, there is a clear interface between the W, Cu, and Ni phases, as well as W exfoliation. After heat treatment, the interface becomes blurred and the peeling phenomenon of W particles is suppressed. As shown in Fig. S7, Cu and Ni interdiffuse to create a solid solution of Cu0.81Ni0.19. The metallurgical bonding between W and Cu is realized when Cu diffuses into the W phase (as shown in Fig. 4(c)). Element doping is responsible for the increased diffusion coefficient [43]. It is also believed that the kinetic energy generated during cold spraying is used to diffuse Cu into the W lattice for solid solution ($\Delta H(Cu \rightarrow W) = 86$ kJ/mol against $\Delta H(W \rightarrow Cu) = 107$ kJ/mol) [44], similar to the solid solubility of W—Cu produced by mechanical alloying. The addition of Ni transition layer and post-treatment are essential to obtain high W content coating. Fig. 5 shows the microstructure of the W—Cu coating before and after heat treatment. After heat treatment at 600 °C, the interdiffusion between Cu and Cu particles eliminates the pore between Cu particles (white arrow). However, the pore (blue arrow) created by the peeling of W particles cannot be eliminated. Fig. 6 shows the microstructure of the W-(Ni)-Cu

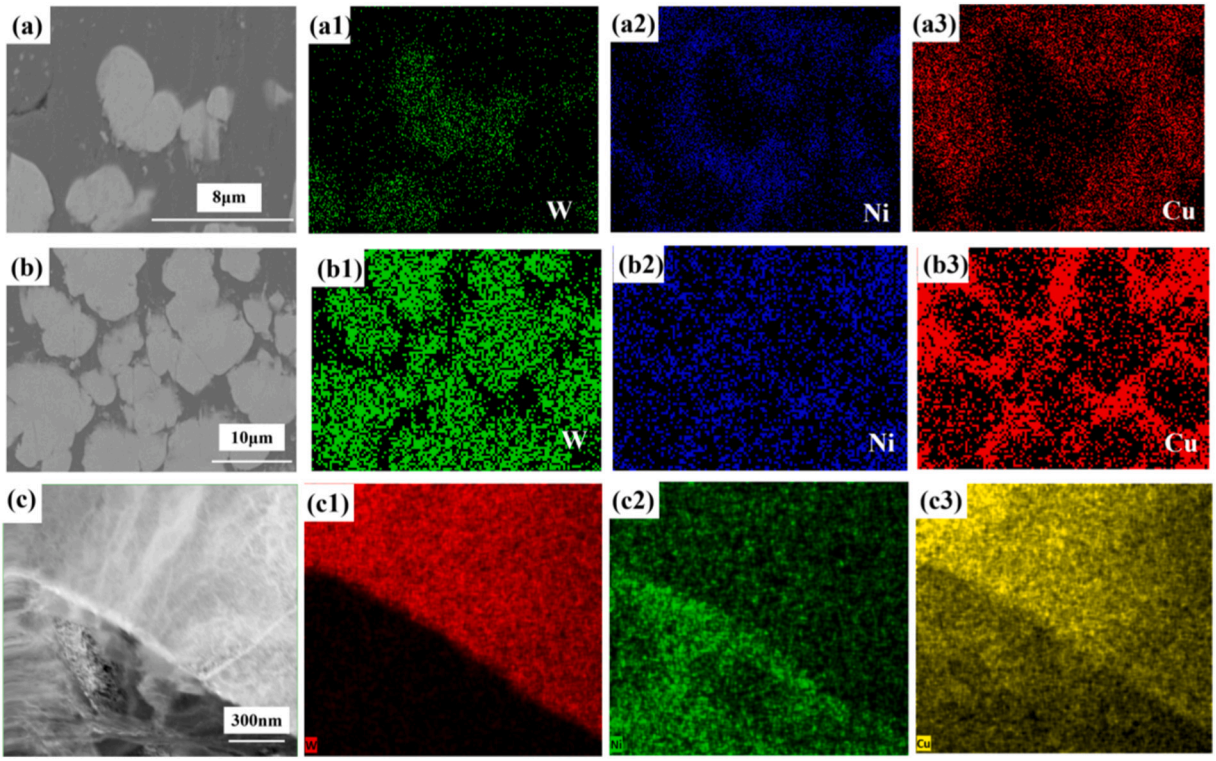

Fig. 4. The SEM images of the W-(Ni)-Cu coating with map scanning (a) before and (b) after heat treatment; (c) High Resolution Transmission Electron Microscope (HRTEM) image and EDS mapping of the W-(Ni)-Cu coating after heat treatment.

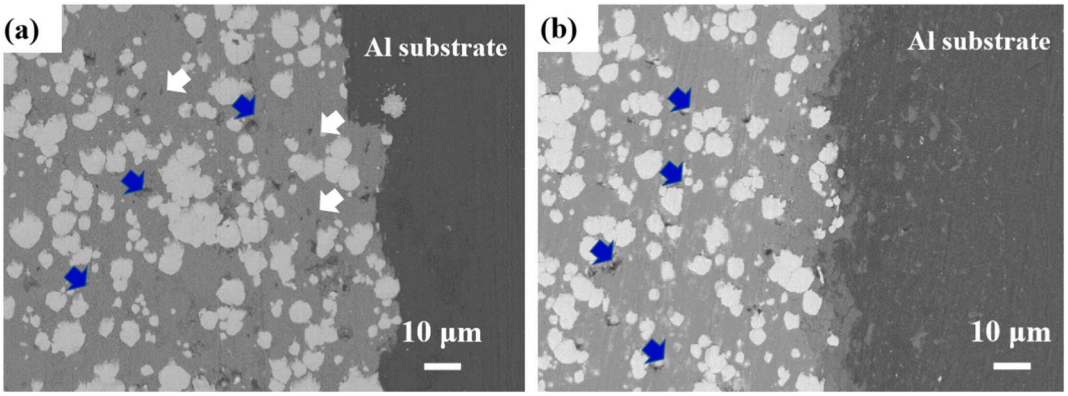

Fig. 5. The microstructure of the W—Cu coating (a) before and (b) after heat treatment 600 °C for 4 h.

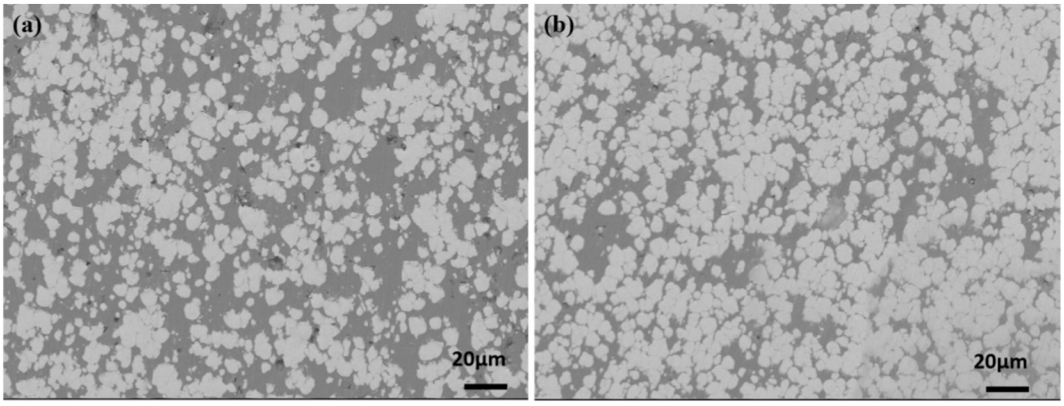

Fig. 6. The SEM images of the W-(Ni)-Cu coating (a) before and (b) after heat treatment 600 °C for 4 h.

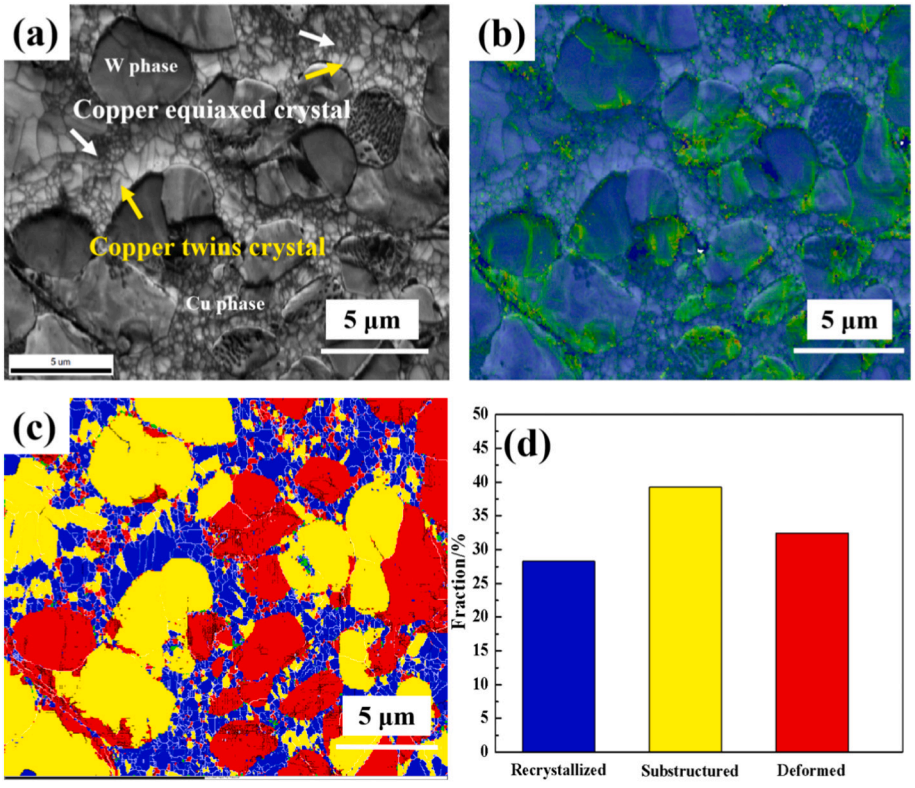

Fig. 7. EBSD images of cross-section of core-shell powders after heat treatment (a) IQ image, (b) KAM image (the degree deformation from blue to green), (c) the distribution of recrystallized (in blue), substructured (in yellow) and deformed (in red) grains in the coating (white line is high-angle grain boundary (HAGB) and black line is high-angle grain boundary (LAGB)) and (d) obtained statistical data (impact direction is from top to bottom). (For interpretation of the references to colour in this figure legend, the reader is referred to the web version of this article.)

coating before and after heat treatment. It is indicated that the pores created by the peeling of W particles are eliminated by adding Ni interlayer and by the heat treatment. Among them, adding Ni transition layer is very important. It can be believed that the existence of Ni element, its doping effect will cause the coating to form a W—Cu solid solution after subsequent heat treatment process, and obtain a good W—Cu interface in the coating.

Furthermore, the kernel average misorientation (KAM) map and collected statistical data corroborate the plastic deformation and recrystallization of the coating (Fig. 7(c, d)). Recrystallization of the deformed Cu shell occurs, with equiaxed crystals and twins (Fig. 7(a)), and the fraction of recrystallized regions is 28.2 % (Fig. 7(d)). According to the formula $\rho_{GND} = \frac{2KAM_{ave}}{\mu b}$, where ρ_{GND} is the average geometrical dislocation density, KAM_{ave} represents local misorientation, μ is EBSD experimental step size, and b is the burges vector. As illustrated in Fig. 7 (b), it represents the degree of plastic deformation. Because of recrystallization, the dislocation density within the Cu phase is lower, resulting in a low local misorientation [45]. The W phase and its interface still have the highest residual plastic deformation (Fig. 7(c)) and have more local misorientations than other locations, suggesting higher dislocation density. These dislocations provide additional locations for Cu atoms to enter the W lattice and form a W—Cu solid solution. The results of EBSD confirm HRTEM results in Fig. 4.

3.3. The porosity of W—Cu composite coatings

Non-localized strain and dispersive residual stresses occur in the sprayed coating, demonstrating low rebound energy and interfacial bonding energy, further allowing W particles to deposit well. As a result, the W@Cu core-shell powder may achieve a high W concentration in the coating. Every layer of the formed coating corresponds to the W and Cu phases. The W@Cu core-shell powder may surround the W phase with the Cu phase, decreasing the possibility of W particles colliding directly. Furthermore, the Cu phase causes plastic deformation, whereas the W phase tamps the coating. The W@Cu core-shell powder may minimize the poor plastic dissipation area produced by W aggregation, which is advantageous in the preparation of high W content coating.

Consequently, X-ray micro-computed tomography was used to identify the porosity of the composite coating, as shown in Fig. 8. The initial W—Cu coating by using W@Cu core-shell powder (without Ni addtion) has a body porosity of 4.6 %. The diameter distribution is 6–8 μm, which is close to the original W powder particle size distribution range. It suggests that the porosity in the initial W—Cu coating is generated by the exfoliation of W particles. The body porosity of the W-(Ni)-Cu coating is decreased to 1 % with the addition of a Ni inter-layer. To guarantee the accuracy of the result, we use several locations to test the body porosity. Although the distribution of bulk porosity is an interesting phenomenon, it is not covered in this work. As shown in Fig. 8(g), the W retention rate in this article is as high as 98.3 %, which is much higher than the value reported in previous works [22,23,39,46–49]. The residual stress generated in the particles upon impact may affect the mechanical, thermal, and electrical characteristics of the coatings. These may be to some extent modified by subsequent heat treatment. Therefore, we will do further study on coating performance enhancement.

4. Conclusion

In conclusion, a W—Cu composite coating with a high W content (fraction of mass, 70 % W versus containing originally 71.2 % W) is cold sprayed by utilizing a novel W@Cu core-shell powder at low pressure (2 MPa, Air-gas), which has not been reported before. The impacting and depositing mechanics are studied using FE simulation. The main FE simulation result is that the W@Cu core-shell powder has a nonlocalized strain and dispersive residual stresses, resulting in low rebound energy and interfacial bonding energy. Therefore, W particles can deposit effectively, which is essential for preparing high W content coating. The retention rate of W in the final coating further increases to 98.3 % with the addition of a Ni inter-layer and the body porosity reduces to 1 %.

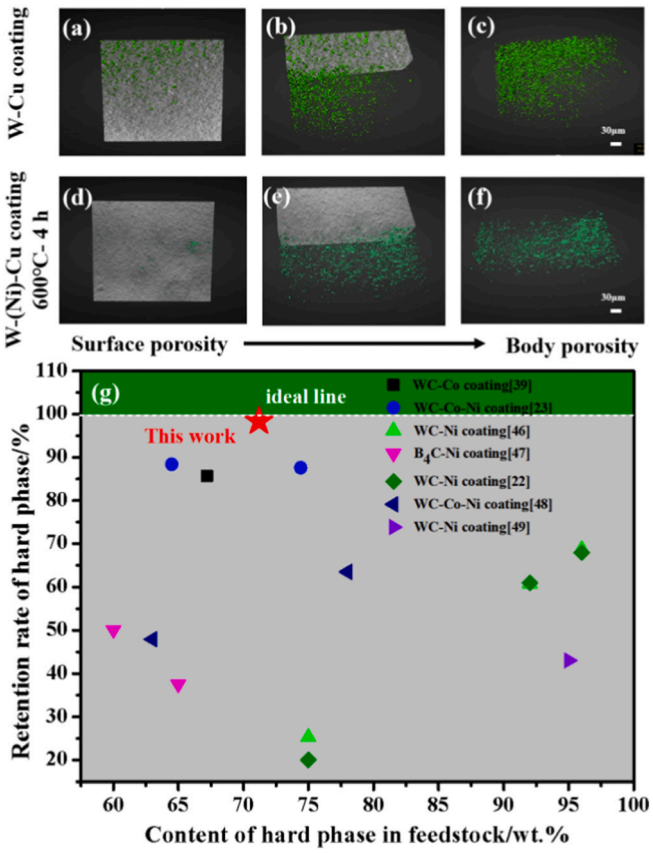

Fig. 8. The porosity of coating (The 3D rendering images obtained by segmenting the internal pores of the sample with Dragonfly software. Left to right: surface porosity to body porosity): (a)-(c) W—Cu composite coating, (d)-(f) W-(Ni)-Cu coating after heat treatment; (g) comparison of retention rate of hard phase in different studies.

CRediT authorship contribution statement

Nan Deng: Conceptualization, Methodology, Investigation, Writing – original draft, Writing – review & editing, Funding acquisition. **Dandan Qu:** Conceptualization, Methodology, Investigation, Writing – original draft, Writing – review & editing, Funding acquisition. **Kun Zhang:** Methodology, Writing – review & editing. **Guoliang Liu:** Methodology, Writing – review & editing. **Shaofu Li:** Methodology, Writing – review & editing. **Zhangjian Zhou:** Conceptualization, Methodology, Writing – review & editing, Funding acquisition, Supervision.

Declaration of competing interest

The authors declare no competing financial interests.

Data availability

The data that has been used is confidential.

Acknowledgement

This work was financially supported by the National Natural Science

Foundation of China (NO. 52204374, NO. 11802309) and the National MCF Energy R&D Program of China (2018YFE0306100). The author thanks C. J. Cao, W. Shi, and X. Sun (Carl Zeiss Microscopy Customer Center, Beijing, China) for the sample mounting method, imaging technology support in the computed micro-X-ray tomography tests, and 3D reconstruction and analysis.

Appendix A. Supplementary data

Supplementary data to this article can be found online at https://doi.org/10.1016/j.surfcoat.2023.129639.

References

[1] T. Han, C. Hou, Z. Zhao, X. Huang, F. Tang, Y. Li, X. Song, W-cu composites with excellent comprehensive properties, Compos. B Eng. 233 (2022), 109664.
[2] A.G. Hamidi, H. Arabi, S. Rastegari, The effect of microstructural aspects of W Cu composites on electrical conductivity and thermal erosion, Int. J. Refract. Met. Hard Mater. 101 (2021), 105685.
[3] C. Hou, X. Song, F. Tang, Y. Li, L. Cao, J. Wang, Z.W. Nie, W-Cu composites with submicron- and nanostructures: progress and challenges, in: NPG Asia Mater 11, 2019, p. 74.
[4] H. Zhang, J. Liu, G. Zhang, Preparation and properties of W-30 wt% Cu alloy with the additions of Ni and Fe elements, J. Alloy Compd. 928 (2022), 167040.
[5] D. Liu, M. Lin, J. Zou, L. Luo, Y. Wu, Microstructure and properties of silver-added W-Cu prepared by infiltration sintering, Int. J. Refract. Met. Hard Mater. 108 (2022), 105947.
[6] R.N. Raoelison, C. Verd, H. Liao, Cold gas dynamic spray additive manufacturing today deposit possibilities, technological solutions and viable applications, Mater. Des. 133 (2017) 266–287.
[7] A.P. Alkhimov, V.F. Kosarev, A.N. Papyrin, A method of cold gas-dynamic spraying, Dokl. Akad. Nauk SSSR 315 (1990) 1062–1065.
[8] H. Assadi, H. Kreye, F. Gärtner, T. Klassen, Cold spraying-a materials perspective, Acta Mater. 116 (2016) 382–407.
[9] H.G. Mostafa, V. David, V.K. Champagne, K.A. Nelson, C.A. Schuh, Adiabatic shear instability is not necessary for adhesion in cold spray, Acta Mater. 158 (2018) 430–439.
[10] H. Assadi, F. Gärtner, T. Klassen, H. Kreye, Comment on 'adiabatic shear instability is not necessary for adhesion in cold spray, Scr. Mater. 182 (2019) 512–514.
[11] H.G. Mostafa, V. David, V.K. Champagne, K.A. Nelson, C.A. Schuh, Response to comment on "adiabatic shear instability is not necessary for adhesion in cold spray", Scr. Mater. 162 (2019) 515–519.
[12] R.C. Dykhuizen, M.F. Smith, D.L. Gilmore, R.A. Neiser, X. Jiang, S. Sampath, Impact of high velocity cold spray particles, J. Therm. Spray Technol. 8 (1999) 559–564.
[13] K. Yokoyama, M. Watanabe, S. Kuroda, Y. Gotoh, T. Schmidt, F. Gartner, Simulation of solid particle impact behavior for spray processes, Mater. Trans. 47 (2006) 1697–1702.
[14] T. Schmidt, F. Gartner, H. Assadi, H. Kreye, Development of a generalized parameter window for cold spray deposition, Acta Mater. 54 (2006) 729–742.
[15] G. Bae, Y. Xiong, S. Kumar, K. Kang, C. Lee, General aspects of interface bonding in kinetic sprayed coatings, Acta Mater. 56 (2008) 4858–4868.
[16] J. Xie, D. Nelias, B.H. Walter-Le, Y. Ichikawa, K. Ogawa, Numerical simulation of the cold spray deposition process for aluminium and copper, in: Proceedings of the ASME 2012 11th Biennial Conference on Engineering Systems Design and Analysis, 2012 (Nantes, France).
[17] H. Assadi, F. Gärtner, T. Stoltenhoff, H. Kreye, Bonding mechanism in cold gas spraying, Acta Mater. 51 (2003) 4379–4394.
[18] R.C. Dykhuizen, M.F. Smith, Gas dynamic principles of cold spray, J. Therm. Spray Techn. 7 (2) (1998) 205–212.
[19] H.J. Kima, C.H. Lee, S.Y. Hwang, Fabrication of WC-Co coatings by cold spray deposition, Surf. Coat. Tech. 191 (2005) 335–340.
[20] B. Giovanni, D. Sergi, L. Luca, M. Tiziano, J.M. G, I.G. C, Building up WC-Co coatings by cold spray: a finite element simulation, Surf. Coat. Tech. 374 (2019) 674–689.
[21] H.Y. Lee, Y.H. Yu, Y.C. Lee, Y.P. Hong, K.H. Ko, Cold spray of SiC and Al_2O_3 with soft metal incorporation: a technical contribution, J. Therm. Spray Technol. 13 (2) (2004) 184–189.
[22] H.K. Kang, S.B. Kang, Tungsten copper composite deposits produced by a cold spray, Scr. Mater. 49 (2003) 1169–1174.
[23] N.M. Melendez, A.G. Mcdonald, Development of WC-based metal matrix composite coatings using low pressure cold gas dynamic spraying, Surf. Coat. Technol. 214 (2013) 101–109.
[24] N.M. Melendez, V.V. Narulkar, G.A. Fisher, Effect of reinforcing particles on the wear rate of low pressure cold-sprayed WC-based MMC coatings, Wear 306 (2013) 185–195.
[25] N. Deng, J.R. Tang, T.Y. Xiong, J.Q. Li, Z.Z. Zhou, Fabrication and characterization of W-Cu composite coatings with different W contents by cold spraying, Surf. Coat. Technol. 368 (2019) 8–14.
[26] K.S. Al-Hamdani, J.W. Murray, T. Hussain, A. Kennedy, A.T. Clare, Cold sprayed metal–ceramic coatings using satellited powders, Mater. Lett. 198 (2017) 184–187.
[27] S. Yin, Y.C. Xie, J. Cizek, E.J. Ekoi, T. Hussain, D.P. Dowling, R. Lupoi, Advanced diamond–reinforced metal matrix composites via cold spray: properties and deposition mechanism, Compos. B Eng. 113 (2017) 44–54.
[28] C.J. Huang, W.Y. Li, Y.C. Xie, M.P. Planche, H. Liao, G. Montavon, Effect of substrate type on deposition behavior and wear performance of Ni-coated graphite-Al composite coatings deposited by cold spraying, J. Mater. Sci. Technol. 33 (4) (2017) 338–346.
[29] X.L. Xie, C.Y. Chen, Y.C. Xie, Z. Ren, E. Aubry, G. Ji, H. Liao, A novel approach for fabricating Ni-coated FeSiAl soft magnetic composite via cold spraying, J. Alloy Compd. 749 (2018) 523–533.
[30] S. Yin, J. Cizek, C. Chen, R. Jenkins, R. Lupoi, Metallurgical bonding between metal matrix and core-shelled reinforcements in cold sprayed composite coating, Scr. Mater. 177 (2019) 49–53.
[31] P. Petrovskiy, M. Doubenskaia, A. Sova, A. Travyanov, Analysis of copper-tungsten cold spray coating: kinetics of coating formation and its thermal properties, Surf. Coat. Technol. 385 (2020), 125376, https://doi.org/10.1016/j.surfcoat.2020.125376.
[32] Lewei He, David Veysset, Isaac M. Nault, Victor K. Champagne, Mostafa Hassani, Impact and bonding behavior of core-shell powder particles, Surf. & Coat. Technol. 441 (2022), 128591.
[33] Baran Yildirim, Hirotaka Fukanuma, Teiichi Ando, Andrew Gouldstone, Sinan Mueftue, A numerical investigation into cold spray bonding processes, J. Tribol. 137 (2015), 011102.
[34] C. Hamilton, A. Sommers, S. Dymek, A thermal model of friction stir welding applied to Sc-modified Al–Zn–Mg–Cu alloy extrusions, Int J Mach Tool Manu 49 (2009) 230–238.
[35] Erik Lassner, Wolf-Dieter Schubert, Tungsten Properties, Chemistry, Technology of the Element, Alloys, and Chemical Compounds, Kluwer Academic/Plenum Publishers, 1998.
[36] G. Bae, Y. Xiong, S. Kumar, K. Kicheol, L. Changhee, General aspects of interface bonding in kinetic sprayed coatings, Acta Mater. 56 (17) (2008) 4858–4868.
[37] Baran Yildirim, Hirotaka Fukanuma, Teiichi Ando, Andrew Gouldstone, M. Sinan, A numerical investigation into cold spray bonding processes, J. Tribol-T Asme 137 (2015) 1–13.
[38] S. Yin, J. Cizek, C. Chen, R. Jenkins, G. O'Donnell, R. Lupoi, Metallurgical bonding between metal matrix and core-shelled reinforcements in cold sprayed composite coating, Scr. Mater. 177 (2020) 49–53.
[39] X.T. Luo, C.X. Li, F.L. Shang, G.J. Yang, Y.Y. Wang, C.J. Li, WC-Co composite coating deposited by cold spraying of a core–shell–structured WC-Co powder, J. Therm. Spray Technol. 24 (1–2) (2015) 100–107.
[40] K. Yang, W.Y. Li, X.P. Guo, X. Yang, Y. Xu, Characterizations and anisotropy of cold–spraying additive–manufactured copper bulk, J. Mater. Sci. Technol. 34 (09) (2018) 118–127.
[41] R. Huang, M. Sone, W.H. Ma, H. Fukanuma, The effects of heat treatment on the mechanical properties of cold-sprayed coatings, Surf. Coat. Technol. 261 (2015) 278–288.
[42] P.D. Eason, J.A. Fewkes, S.C. Kennett, T.J. Eden, K. Tello, M.J. Kaufman, M. Tiryakioglu, On the characterization of bulk copper produced by cold gas dynamic spray processing in as fabricated and annealed conditions, Mater. Sci. Eng. A Struct. 528 (28) (2011) 8174–8178.
[43] J. Cui, S.H. Liang, Y. Wei, X.H. Wang, Diffusion behavior of W in the WCu/Ni interface, Int. J. Refract. Met. Hard Mater. 29 (2) (2011) 153–157.
[44] A.R. Miedema, P.F. Chatel, F.R. Boer, Cohesion in alloying-fundamentals of semi-empirical model, Physics 100B (1) (1980) 1–28.
[45] P.F. Yu, N.S. Fan, Y.Y. Zhang, Z.J. Wang, W.Y. Li, R. Lupoi, S. Yin, Microstructure evolution and composition redistribution of FeCoNiCrMn high entropy alloy under extreme plastic deformation, Mater. Res. Lett. 10 (3) (2022) 124–132.
[46] Y. Shuo, J.E. Emmanuel, L.L. Thomas, D.P. Dowling, R. Lupoi, Cold spraying of WC–Co–Ni coatings using porous WC–17Co powders: formation mechanism, microstructure characterization and tribological performance, Mater. Des. 126 (2017) 305–313.
[47] C. Feng, V. Guipont, M. Jeandin, O. Amsellem, F. Pauchet, R. Saenger, S. Bucher, C. Iacob, B_4C-Ni composite coatings prepared by cold spray of blended or CVD-coated powders, J. Therm. Spray Technol. 21 (3–4) (2012) 561–570.
[48] D. Lioma, N. Sacks, I. Botef, Cold gas dynamic spraying of WC-Ni cemented carbide coatings, Int. J. Refract. Met. Hard Mater. 49 (2015) 365–373.
[49] P. Nunthavarawong, N. Sacks, I. Botef, Effect of powder feed rate on the mechanical properties of WC-5 wt%Ni coatings deposited using low pressure cold spray, Int. J. Refract. Met. Hard Mater. 61 (2016) 230–237.